To the Graduate Council:

I am submitting herewith a thesis written by Michael Glenn Anderson entitled "The Effects of Energy Dependence on Radiographs." I have examined the final copy of this thesis for form and content and recommend that it be accepted in partial fulfillment of the requirements for the degree of Master of Science, with a major in Electrical Engineering.

L. Montgomery Smith

L. Montgomery Smith, Major Professor

We have read this thesis
and recommend its acceptance:

Roy D Joseph

Richard M. Rotenda

W K McGregor

Accepted for the Council:

Lawrence

Associate Vice Chancellor
and Dean of The Graduate School

STATEMENT OF PERMISSION TO USE

In presenting this thesis in partial fulfillment of the requirements for a Master's degree at The University of Tennessee, Knoxville, I agree that the Library shall make it available to borrowers under rules of the Library. Brief quotations from this thesis are allowable without special permission, provided that accurate acknowledgment of the source is made.

Permission for extensive quotation from or reproduction of this thesis may be granted by my major professor, or in his absence, by the Head of Interlibrary Services when, in the opinion of either, the proposed use of the material is for scholarly purposes. Any copying or use of the material in this thesis for financial gain shall not be allowed without my written permission.

Signature Michael G. Collins

Date 2 Dec 92

THE EFFECTS OF ENERGY DEPENDENCE ON RADIOGRAPHS

A Thesis

Presented for the

Master of Science

Degree

The University of Tennessee, Knoxville

Michael Glenn Anderson

December 1992

ACKNOWLEDGMENTS

I would like to thank my major professor, Dr. Monty Smith, for his guidance and patience. I would also like to thank the other committee members, Dr. Wheeler McGregor, Dr. Richard Roberds, and Dr. Roy Joseph for their comments and assistance over the past year. I would like to express my thanks to my father, Ernest Anderson, for his encouragement to continue my education. This work was performed at Arnold Engineering Development Center at Arnold Air Force Base, Tennessee under project number DB90.

ABSTRACT

The objective of this work was to ascertain the effects of energy dependence on X-ray radiographs for real-time radiography applications. More specifically, it was to determine if this energy dependence must be considered in accurately predicting radiographs. The energy dependent characteristics of the x-ray source, the object being radiographed, and the x-ray-to-light conversion screens were considered. The energy dependence of the source was characterized analytically and was also characterized experimentally but with limited success. The effects were explored by first simulating a one dimensional intensity profile of a radiograph assuming no energy dependence, i.e., the monochromatic condition, and then simulating the profile assuming the polychromatic condition. These two profiles were then compared to a profile derived from an actual radiograph taken under similar conditions. The results showed that the polychromatic prediction more closely resembled the actual radiograph than did the monochromatic prediction for this test case. This was the case because the effective energy of the x-rays vary as a function of the path length through the object and because the monochromatic assumption was unable to account for the effects of the intensifying screens in the imaging process.

TABLE OF CONTENTS

LIST OF FIGURES

NOMENCLATURE

μ	attenuation coefficient
A	atomic weight
ADC	analog to digital converter
c	speed of light
CsI	cesium iodide
E	energy
E_k	kinetic energy
FET	field-effect transistor
f_{KN}	Klein Nishina number
Ge	germanium
h	Planck's constant
I	intensity
i	current
I_b	binding energy
I_f	final photon intensity
I_o	initial photon intensity
KeV	kilo electron volts
KV	kilovolts
LED	light-emitting diode
Li	lithium
LN2	liquid nitrogen
MCA	multichannel analyzer
m_e	mass of an electron
MeV	million electron volts

MHz	mega hertz
Mono.c	monochromatic raytrace program
n_e	number of electrons
N_o	Avagadro's number
PHA	pulse height analysis
Poly.c	polychromatic raytrace program
Si	silicon
Si(Li)	lithium drifted silicon detector
V	voltage
x	distance through an object
Z	atomic number
υ	frequency
λ	wavelength
σ	cross section
ρ	density
μ	linear attenuation coefficient
μ_c	attenuation coefficient due to Compton effect
μ_{pe}	attenuation coefficient due to photoelectric effect
°K	degrees Kelvin

I. INTRODUCTION

X-ray radiography has been extensively used in both medical and industrial applications to view the internal structures of various objects. X-ray photons are generated and are passed through a three dimensional object which attenuates the photons based on the physical properties of the object. These photons are then absorbed by a medium to form a two dimensional image of the object. This medium can either be film, or in the case of real-time radiography, can be a fluorescing material (screen) which emits visible light upon absorbing the x-ray photons. This visible light is, in turn, viewed by a video camera and the image is recorded on video tape. A basic layout of a real-time system is shown in Figure 1.

Several authors [1] [2] [3] have presented methods to predict the resulting radiographs. This prediction is useful for two reasons. The first is as an aid in the layout, selection, and operating conditions for the equipment in taking an actual radiograph. The second concerns the analysis of actual radiographs. For example, if the film density, or video gray level, of a pixel in the image is known, the object thickness can be calculated. The complexity and accuracy of image prediction is a function of the assumptions made about the

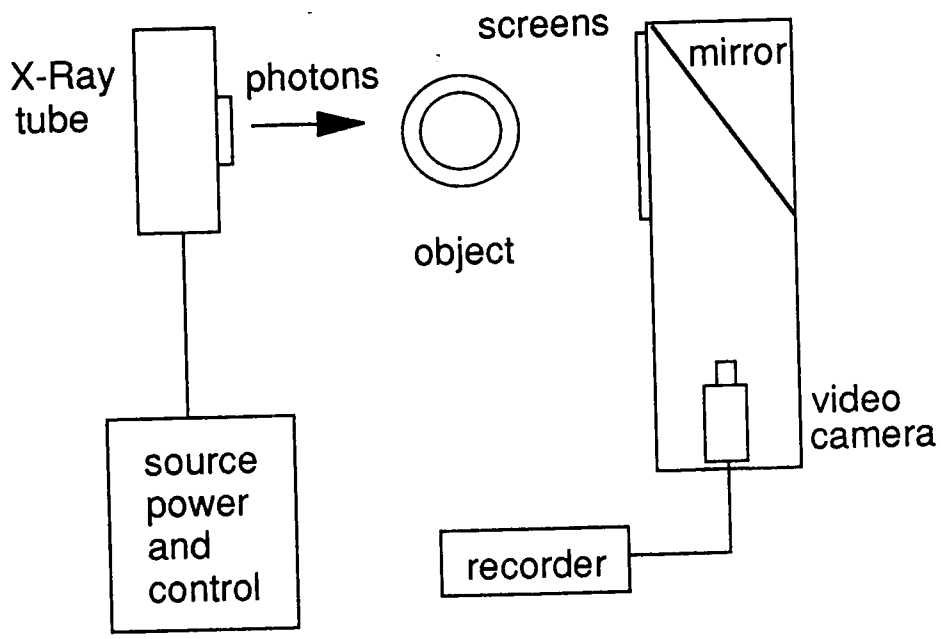

Figure 1. Basic Layout of a Real-time Radiography System

radiographic imaging process. A major part of these assumptions relate to the energy or photon wavelength dependence of the following:

(1) x-ray source output intensity spectrum
(2) object attenuation characteristics
(3) imaging medium screen absorption properties

Frederick and Williams [1] made predictions of a two dimensional video image for real-time applications, assuming the monochromatic case in which all of the three parameters above were assumed to be constant. Laguna [2] made predictions for film applications, assuming a partially polychromatic case. The source output and object attenuation were energy dependent, but the screen or film characteristics were assumed to be constant with energy. The source output Laguna used was a spectrum obtained from an x-ray tube operating at an energy of 30 kilovolts (KV). Siewert et. al. [3] made one dimensional profile predictions using monochromatic assumptions for the purpose of evaluating a new type of spherical penetrameter to make radiographic sensitivity measurements.

This work attempts to find how significant the energy dependence is in predicting the radiograph. Must the energy dependence be considered, and if so, how, or is the

monochromatic assumption sufficient?

The approach taken first involved experimentally taking a video radiograph of a test object, a hollow aluminum cylinder. Aluminum was chosen because it is a material commonly radiographed in industrial applications, e.g., wheel castings. A video frame was digitized and from this a one dimensional intensity, or image gray level profile was taken through the center of the object. Figure 2 shows the relationship between the object geometry and the general shape of the resulting one dimensional profile. The experimentally derived profile was compared to profiles predicted by two computer models. For the first model, Mono.c, the profile was calculated assuming the totally monochromatic case. For the second, Poly.c, the profile was calculated assuming the polychromatic case, i.e., all three of the above parameters were energy dependent. The energy dependence of the x-ray source output was characterized experimentally, using an x-ray spectrometer, and analytically, using Kramer's formula for the continuum as a function of the source operating parameters. Comparison of the profiles with the experimental profile showed that the intensity profile using the polychromatic predictions more closely resembled the profile derived from the actual radiograph.

In this work the background theory necessary for

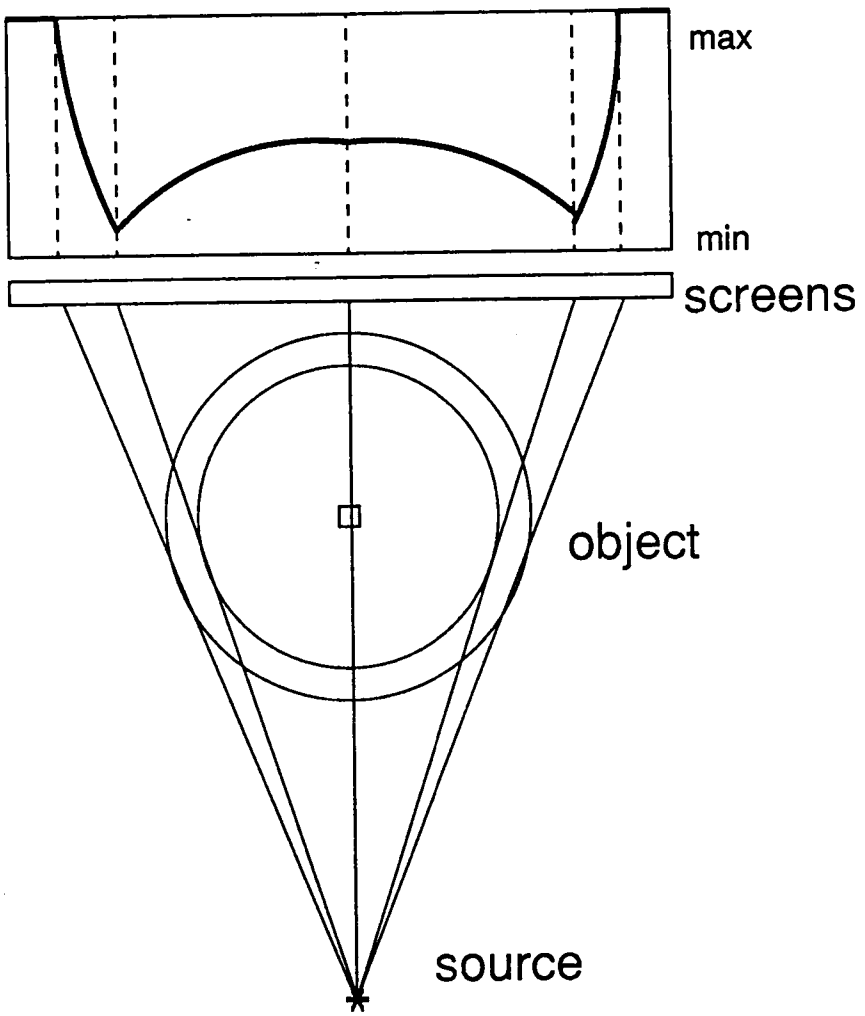

Figure 2. Correlation of Intensity Profile to the Source, Object, and Screen Layout

understanding the radiographic process will be first discussed. Secondly, the method to experimentally derive source spectral data and acquiring the radiographic image data are described. The monochromatic and polychromatic prediction models are then discussed in some detail. Finally, the experimental and predicted intensity profiles are compared and discussed and reasons given as to why the polychromatic case yielded a more accurate prediction.

II. BACKGROUND

As mentioned above, the following energy dependent parameters affect the radiograph:

(1) x-ray source output intensity spectrum

(2) object of interest attenuation characteristics

(3) imaging medium, e.g., intensifying screen absorption efficiency.

These are discussed in detail in the following.

A. X-RAY SOURCE OUTPUT

X-ray sources used for radiography vary in energy from several kiloelectron volts (KeV) to several million electron volts (MeV) and are in the form of tubes, linear accelerators, or isotopes, depending on the specific application. The energy range of interest in this work was below 320 KeV, where the sources are generally x-ray tubes. An X-ray tube generates x-rays by emitting electrons from a filament (cathode), accelerating them across a potential, and impinging them on a target material (anode). The x-rays generated consist of both a continuum of radiation, or Bremsstrahlung radiation, and of radiation characteristic of the anode material at discrete wavelengths.

1. CONTINUOUS SPECTRA

An x-ray tube produces a continuous spectra of

intensities which is dependent on the tube operating parameters. The continuum is caused by the release of photons when the electrons from a cathode are decelerated in the target material of an anode. When the negatively charged electrons pass close to a nucleus of the target material, the strong attractive Coulomb force causes the electrons to deviate sharply from their original path. The change in direction is due to radial acceleration, and the electrons lose energy by electromagnetic radiation [4]. This radiation in the form of photons has an energy equal to $h\upsilon$ where h is Planck's constant and υ is the frequency, and $h\upsilon$ is the total energy lost by the electron. The amount of energy lost cannot exceed the total energy of the moving electron but can have any value smaller than this. The maximum energy that can be present in the emitted photons is generated when the incident electrons completely decelerate and the energy of the incident electrons is completely transferred into the emitted photons. This maximum energy is therefore directly related to the maximum frequency of the photons by

$$E_{max} = h\upsilon_o = hc / \lambda_{min} \qquad \text{(II.1)}$$

where υ_o is the maximum frequency, with corresponding minimum wavelength λ_{min}, of the emitted x-rays, h is

Planck's constant, and c is the speed of light. Below this maximum frequency, there will be a continuous spectrum of frequencies as a result of electrons losing only part of their energies to the nuclei [5]. The tube operating voltage is related to this maximum energy by:

$$V = 12.4 / \lambda_{min} \qquad \text{(II.2)}$$

where V is the tube operating voltage in KeV and λ_{min} is the minimum wavelength in Angstroms. This is derived directly from the definition of the electron volt. The tube operating voltage alone therefore determines the maximum frequency and thus energy of photons present in the continuous spectrum. Because the number of electrons hitting the target material is directly proportional to the tube current, a change in current causes a proportional change in continuum intensity [6].

2. CHARACTERISTIC SPECTRA

The second type of radiation emitted from the X-ray tube is radiation characteristic of the target material. To illustrate the process, it is adequate to use the Bohr model of the atoms in the target material. This consists of a positively charged nucleus with orbiting electrons at specific energy levels. An incident electron from the tube current can dislodge an electron from an electron shell of the target material if the incident electron possesses at least the binding energy of the target electron. When this

occurs, an electron from a higher energy level must take the place of the ejected electron for the atom to remain in equilibrium. This electron transition is characterized by a discrete loss of energy, accompanied by the emission of a photon having an energy equal to the difference in the initial and final electron energies.

The notation for the characteristic transitions is as follows. The first letter of the transition represents the shell in which the initial vacancy took place and thus what shell the transitioning electron ended up in. K is the innermost shell to the nucleus, L the second, M the third, etc. The second letter indicates how many shells out the electron began the transition where α is one, β is two, γ is three, etc. For example, a Kα transition is from the second to the innermost shell transition. All the selection rules of quantum mechanics apply. A good summary of the selection rules is given in Bertin [6] Table 1.3.

B. THE X-RAY SPECTROMETER

The spectral output of an x-ray source was measured with an x-ray spectrometer. X-ray spectrometers fall into two general categories: wavelength-dispersive and energy-dispersive. In wavelength-dispersive spectrometers, the x-rays are dispersed spatially by crystal diffraction, prior to detection, on the basis of their wavelengths [6]. In

energy-dispersive spectrometers, a detector receives all energies of the incoming beam simultaneously and the detector output depends explicitly on the energy of the photons [6]. This work used an energy-dispersive x-ray spectrometer. The major components of an energy dispersive x-ray spectrometer are discussed in the following.

1. DETECTORS

Several types of detectors can be used in an energy-dispersive x-ray spectrometer. In each type, absorbed x-ray photons are converted into pulses of electric current having amplitudes proportional to the photon energy [6]. In all types of detectors, each absorbed photon expels a photoelectron from an atom in the detector. The photoelectron has a kinetic energy equal to the photon energy minus the binding energy of the electron. If this photoionization occurs in the outermost shells of the detector atoms where the binding energy is small compared to the photon energies, the photon can be considered to transfer almost all its energy to the photoelectron. Three of the main types are gas-filled proportional counters, scintillation counters, and solid-state semiconductors. This work used a solid-state semiconductor detector.

Semiconductors are generally poor conductors of electrical current. The use of semiconductors as x-ray detectors rests on absorption of radiation in the material

and the effective ionization of the material, making it momentarily conducting. A bias voltage is placed on the semiconductor crystal. The incoming photons ionize the detector atoms resulting in electron-hole pairs. The absorption of ionizing radiation creates an amount of free charge which ideally is proportional to the photon energy. This free charge is then swept out by the bias voltage as a charge pulse. These detectors generally have a high resolution because there are a large number of electron-hole pairs resulting from a given energy deposit, yielding good statistical definition of the size of the charge pulse.

The crystal used must meet two requirements to be a useful detector. First, the crystal must be very pure to avoid impurity atoms from combining with the lattice atoms to yield free charge carriers and thus increase conductivity. The second is that the crystal should have a high absorption to make an efficient detector. So generally, the higher the atomic number of the detector, the better the absorber. The two semiconductors used presently which best meet the above requirements are silicon (Si) and germanium (Ge). To compensate for the difficulty in manufacturing thick, high-quality detectors, certain impurities are deliberately "drifted" into the material to neutralize the effects of any undesired

impurities. This drifted impurity is usually lithium (Li). The resulting nomenclature of a common detector is lithium drifted silicon or Si(Li).

The detectors are often cooled with liquid nitrogen ($77^{o}K$) to limit the effects of thermally generated charge carriers. This also maintains the lithium compensation because the lithium is relatively mobile in the semiconductor at room temperature, and is especially mobile in the germanium. To help alleviate the problem of the lithium being mobile and its local concentrations changing, high purity germanium detectors were developed, but the germanium has other difficulties associated with it. One problem is the presence of escape peaks in the spectrum. When the x-ray is absorbed in the detector, it will generate a silicon or germanium characteristic x-ray that is again reabsorbed. However, there is the possibility that the x-ray will escape from the detector. The Si $K\alpha$ line is at 1.74 KeV and the Ge $K\alpha$ is at 9.87 KeV. The energy spectrum then read by the detector will be E - $EK\alpha$ and will show up as a separate peak from the parent line and displaced in energy by $EK\alpha$. The problem is greater for the germanium because of the higher $K\alpha$ energy. There is also a large detector efficiency discontinuity at the germanium absorption edge at 11.1 KeV which may be an important part of the spectrum being

measured. The absorption edge is the minimum photon energy that can expel an electron from a specified orbital in an atom of a specified element [6]. The second advantage that the pure germanium detector has is that it has a greater efficiency than the Si(Li) because of a strong absorption dependence on atomic number. In light of these characteristics, Si(Li) is generally used at the lower energies (below 40 KeV) and pure germanium is used exclusively at the higher energies (over 100 KeV) [7].

2. PREAMPLIFIER

The purpose of the preamplifier is to integrate the current conducted by the detector and convert it to a voltage which is proportional to the energy deposited. The preamplifier uses a pulsed optical field-effect transistor (FET). This eliminates the need for a feedback resistor in the amplifier which is a great source of electrical noise. The FET stage builds up a charge equivalent to a tolerable voltage shift, at which a light-emitting diode (LED) is triggered which shines on the FET drain-gate junction and resets the FET [7]. The output of the preamplifier is a voltage sawtooth representing the detector and FET leakage current, upon which are superimposed step increases. The magnitude of each step is proportional to the integrated current conducted by the detector for each x-ray absorption event [8].

3. AMPLIFIER

The function of the amplifier is to take the step increases on the signal out of the preamplifier, and condition the signal for input into the multichannel analyzer (MCA). This involves an initial differentiation and subsequent multiple integrations of the step signal to reduce the effects of signal noise. The output of the amplifier is a bell-shaped voltage pulse, the height of which corresponds to the magnitude of the step input and therefore the photon energy [8].

4. MULTICHANNEL ANALYZER

The final piece of equipment in the x-ray spectrometer is the multichannel analyzer (MCA). Since the voltage pulse height from the amplifier is proportional to the energy of the incoming photon, the MCA performs a pulse-height analysis (PHA) by measuring the height of the pulse and assigning it to a channel number. The number of counts for that channel is then increased by one count. The relative intensity of different spectra can be compared by acquiring the spectra for a constant time. This time must be live-time versus elapsed time. The total elapsed time contains a dead-time. In the amplifiers and MCA there are dead-times associated with several processes such as (1) the preamplifier FET reset time (2) the analog-to-digital converter (ADC) conversion time and (3)

the times the MCA rejects pulses arriving too near to each other in time. Therefore the comparison of the relative intensities of different spectra must be compared with system live-time [7]. The MCA used in this work kept track of its own elapsed-time and live-time.

C. OBJECT ATTENUATION

As the x-ray beam of photons pass through the object being radiographed, the beam is attenuated by both scattering and absorption. In the monochromatic case, this attenuation through the material is characterized by Beer's law:

$$I_f = I_o \exp(-\mu x) \qquad \text{(II.3)}$$

where: I_o is the initial photon intensity

I_f is the final photon intensity

x is the distance traveled through the object

μ is the linear attenuation coefficient of the particular material.

More generally, for the polychromatic case, Beer's law becomes:

$$I_f(E) = I_o(E) \exp[-\mu(E)x] \qquad \text{(II.4)}$$

where the intensities and attenuation coefficient are all energy (E) dependent. In the energy ranges commonly used in radiography, the incident beam is attenuated in three ways: photoelectric absorption, Compton scattering, and

pair production. The total linear attenuation coefficient for the object is the sum of the coefficients due to each of the three processes [9].

1. PHOTOELECTRIC EFFECT

In a photoelectric event, the absorbing atom is ionized by an incident photon and imparts its energy to an ejected photoelectron. The incident photon interacts with an electron whose binding energy, I_b, is less than the energy of the photon, $h\upsilon_o$. The ejected photoelectron has a kinetic energy E_k. The conservation of energy requires that

$$h\upsilon_o = E_k + I_b \qquad \text{(II.5)}$$

The energy of the photoelectron is then dissipated into the absorbing medium [4]. Experimentally it was found that the attenuation coefficient due to the photoelectric effect (μ^{pe}) varies as $Z^4/(h\upsilon_o)^3$ [9], where Z is the atomic number of the material. So in general, for a given material, the photoelectric effect is more pronounced at lower energies and at a given energy, the absorption is greater for higher Z materials.

The $Z^4/(h\upsilon_o)^3$ relationship does not completely characterize the absorption. For any given material, the absorption versus energy relationship exhibits discontinuities called absorption edges. These are due to

the different binding energies, I_b, for the various electron levels. Generally, the attenuation coefficient, or stopping power of the material, decreases as the energy increases. Only x-rays having energy greater than the specified absorption edge are sufficiently energetic to expel electrons from the corresponding level [6]. Figure 3 shows the energy dependence of the mass attenuation coefficient for lead. The mass attenuation coefficient is in units of square centimeters per gram and is equal to the linear attenuation coefficient of Equation II.4 divided by the density. If the energy is assumed to be monochromatic, and it is increased up to energy E1, the material exhibits a certain attenuation μ1. When the energy is increased above E1, but is below E2, the attenuation is actually greater than μ1, because the energy is sufficiently high to interact with electrons from the corresponding shell. It is only when the energy is greater than E2 that the attenuation falls below μ1.

2. COMPTON SCATTERING

Compton scattering is an elastic collision between an incident photon and a free electron whose binding energy is very much less than the energy of the photon [4]. This results in a scattered photon and recoil electron. The scattered photon has less energy, or a longer wavelength than the incident photon.

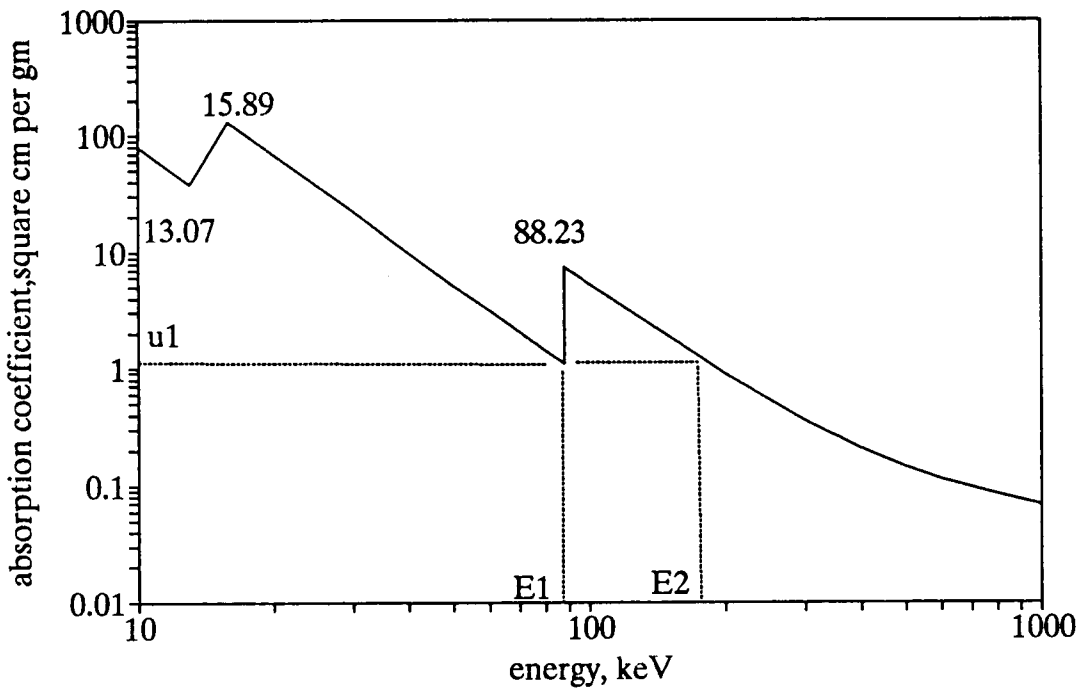

Figure 3. Absorption Coefficient of Lead

If there are n attenuators per unit volume, each with a cross sectional area σ, a very thin slab of thickness dx will remove a fraction $n\sigma dx$ of the incident photons from the beam. If I_o is the incident photon flux (photons/volume), and I(x) is the flux after traveling a distance x, Beer's law, neglecting energy dependence, states as before:

$$I(x) = Io \exp(-\mu x) \tag{II.6}$$

Taking the derivative of this with respect to x yields:

$$\frac{dI(x)}{dx} = (Io)(-\mu) \exp(-\mu x) \tag{II.7}$$

Therefore:

$$\frac{dI(x)}{dx} = -\mu\ I(x) \tag{II.8}$$

The fraction of photons removed from the beam by this thin slab is [9]:

$$\frac{-dI(x)}{I(x)} = \mu\ dx \tag{II.9}$$

In this thin layer dx, we equate the probability of

scattering with the fraction of the beam that is blocked by the attenuators, n_c [9]:

$$\text{probability} = \frac{-dI(x)}{I(x)} = \mu c \quad dx = nc \quad \sigma c \quad dx \qquad \text{(II.10)}$$

where c denotes the effects due to Compton scattering. The photons are scattered by individual electrons so $n_c = n_e$, where n_e is the number of electrons. The electron density in the material is n_e, is given by:

$$ne = No\ Z\ \rho/A \qquad \text{(II.11)}$$

Where N_o is Avagadro's number or the number of atoms per mole of the substance, Z is the atomic number, A is the atomic weight, and ρ is the density. Then the attenuation coefficient due to the Compton effect is:

$$\mu c = ne\ \sigma c = No\ \ {}^{Z}/_{A}\ \rho\ \sigma c \qquad \text{(II.12)}$$

From this relationship we see that the probability of the Compton scattering per unit mass of a substance, increases with the ratio (Z/A). This ratio is generally higher for low Z materials and is usually on the order of 0.5.

The other factor of interest is the energy dependence of μ. This is found in the σ_c term. The σ_c term has been quantified by Klein and Nishina as given in Barrett [9]. It is expressed as:

$$\sigma c = \sigma o \, fKN(\alpha) \qquad \text{(II.13)}$$

where σ_o is the cross section for Thompson or classical scattering, f_{KN} is the Klein-Nishina factor and

$$\alpha = \frac{h\upsilon o}{me\ c^2} \qquad \text{(II.14)}$$

where $m_e c^2 = 0.511$ MeV, the rest energy of the electron and $h\upsilon_o$ was the energy of the incident photon. Substituting yields:

$$\mu c = (No\ Z\ \rho/A)\ \sigma o\ fKN(\alpha) \qquad \text{(II.15)}$$

The Klein Nishina function is given by:

$$f_{KN}(\alpha) = \frac{\sigma c}{\sigma_o} = \frac{3}{4}\left[\frac{2(1+\alpha)^2}{\alpha^2(1+2\alpha)} + \frac{\ln(1+2\alpha)}{\alpha}\left(\frac{1}{2} - \frac{1+\alpha}{\alpha^2}\right) - \frac{1+3\alpha}{(1+2\alpha)^2}\right] \qquad \text{(II.16)}$$

which decreases as α increases. Therefore μ_c also decreases as the incident photon energy increases.

To summarize, the attenuation due to Compton scattering results in scattered photons of lower energy, is more prevalent in low Z materials, and decreases as energy increases. Much more detailed information about the small scale events, e.g. scattering angles of the photon and electron, can be found in Barrett [9], but are not discussed further here since they do not greatly affect the radiographic process.

3. PAIR PRODUCTION

The third type of phenomenon in the interactions of photons with the material is pair production. This effect is present only above 1.02 MeV but is mentioned briefly for completeness since radiography is often done at these energies. As a photon passes near a nucleus, it is annihilated and its energy appears as an electron/positron pair. Tippler [10] describes the process as a photon interacting with a negative-energy electron, raising the electron to a positive-energy state (where it appears as a normal electron) and leaving a hole, which appears as a positron. The threshold energy required for the process is 1.02 MeV or two times the particle's rest mass ($m_e c^2$), where m_e is the mass of the electron and c is the speed of light. The probability of the pair production event increases with Z^2 and with energy above the 1.02 MeV threshold.

4. COMBINED EFFECTS

The total attenuation coefficient is the sum of the individual coefficients for the three processes. For a given material, the total attenuation coefficient can be determined as a function of the energy of the incident photons. The shape of the curve for any material is therefore a function of energy, and the material properties: Z, A, and ρ.

III. EXPERIMENTAL DATA ACQUISITION

A. SOURCE SPECTRAL DATA

1. SYSTEM USED

a. EXPERIMENTAL SETUP

The experimental setup for gathering the X-ray spectral data of the source is shown schematically in Figure 4. The main beam of the source was directed up vertically and into the spectrometer. This orientation was necessary because of the orientation of the liquid nitrogen Dewar flask in the spectrometer. The beam was collimated at the detector through a 1/16 inch thick sheet of lead with a 1/8 inch diameter hole in it. A Victoreen® Model 525 ion gauge was used to measure the source output exposure rate in Roentgens per minute and was placed near the hole between the source and the lead. The distance from the target of the source to the beryllium entrance window of the spectrometer was one meter.

b. SOURCE

The source was a VJ Technologies® Model MF-150. It was a constant potential source with a rotating anode tungsten target. It was supposed to operate over the range of 20 to 160 KeV, but actually went up to only 125 KeV. The tube current was adjustable up to 10 mA and had two effective focal spot sizes of 0.3 and 1.2 millimeters (mm)

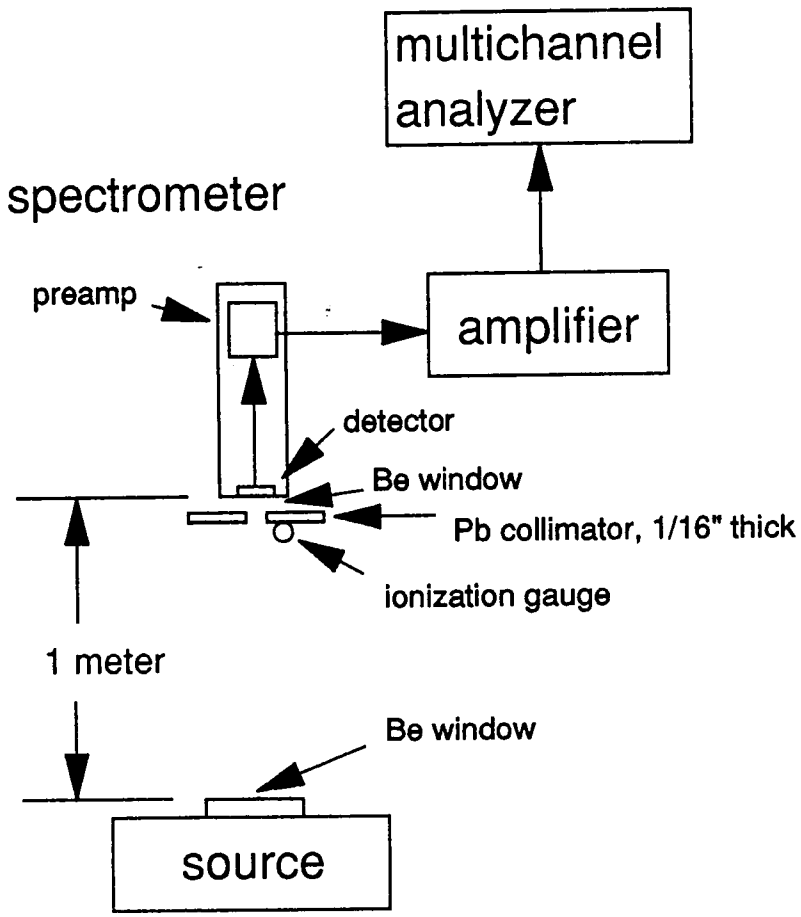

Figure 4. Experimental Setup for Gathering Source Spectral Output

diameters. The spot size is the projected dimension of the electron beam size on the tungsten target.

c. SPECTROMETER

The type of spectrometer used to detect the x-ray spectrum was an energy-dispersive type made by Applied Detector Corporation®. It contained a 25 mm^2, 4 mm thick, pure Germanium, solid state detector. The amplifier used was a Tennelec® TC222 Linear Amplifier and the MCA was a Nucleus® Personal Computer Analyzer (PCA-II™) card in a 80386 computer. The card contained a 100 MHz analog to digital converter (ADC) which digitized the incoming 0 - 8 volt signal into 13 bits or 8192 channels.

2. SPECTRAL DATA RESULTS

Figure 5 illustrates data representative of that taken of the X-ray source using the X-ray spectrometer. The tube parameters for this spectra are 125 KV, 1.49 mA, and 0.75 Roentgens per minute as measured at a distance of one meter from the focal spot. The spectra was gathered over a time period of three seconds. The data from the spectrometer was in the form of counts as a function of channel number. To convert the channel number to energy, a spectra for cobalt-57 radioisotope was taken and is shown in Figure 6. The cobalt-57 has distinctive peaks at 122 KeV (channel 5601) and 136 KeV (channel 6266). Applying this channel to energy relationship to the tube spectrum

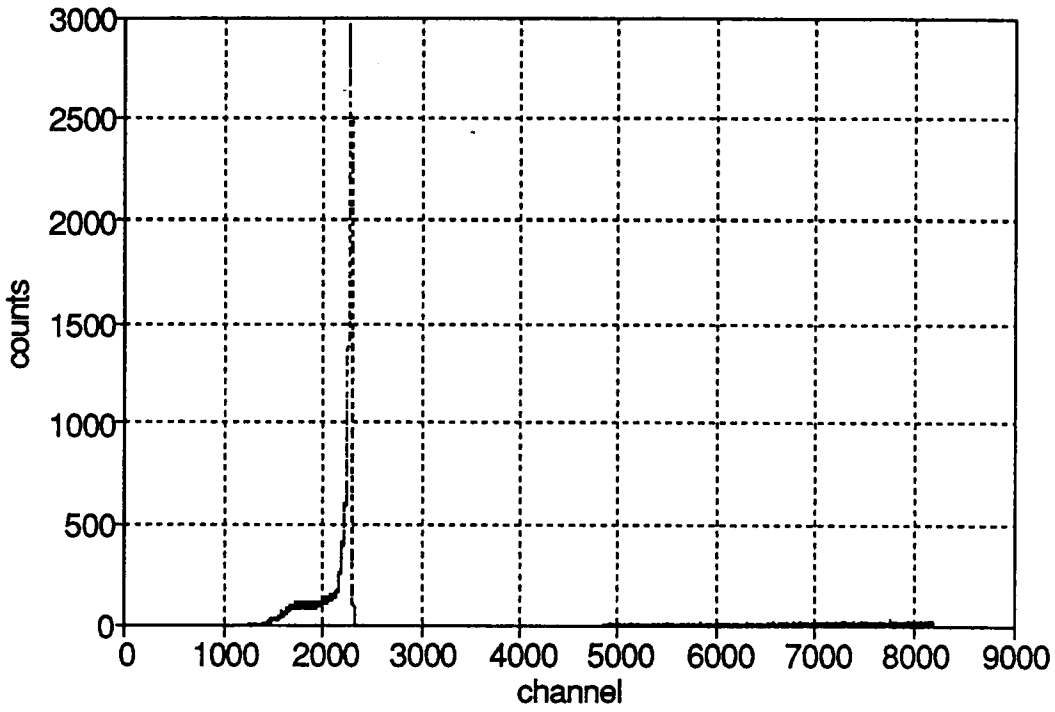

Figure 5. Representative X-ray Spectrometer Data of Source Spectral Output

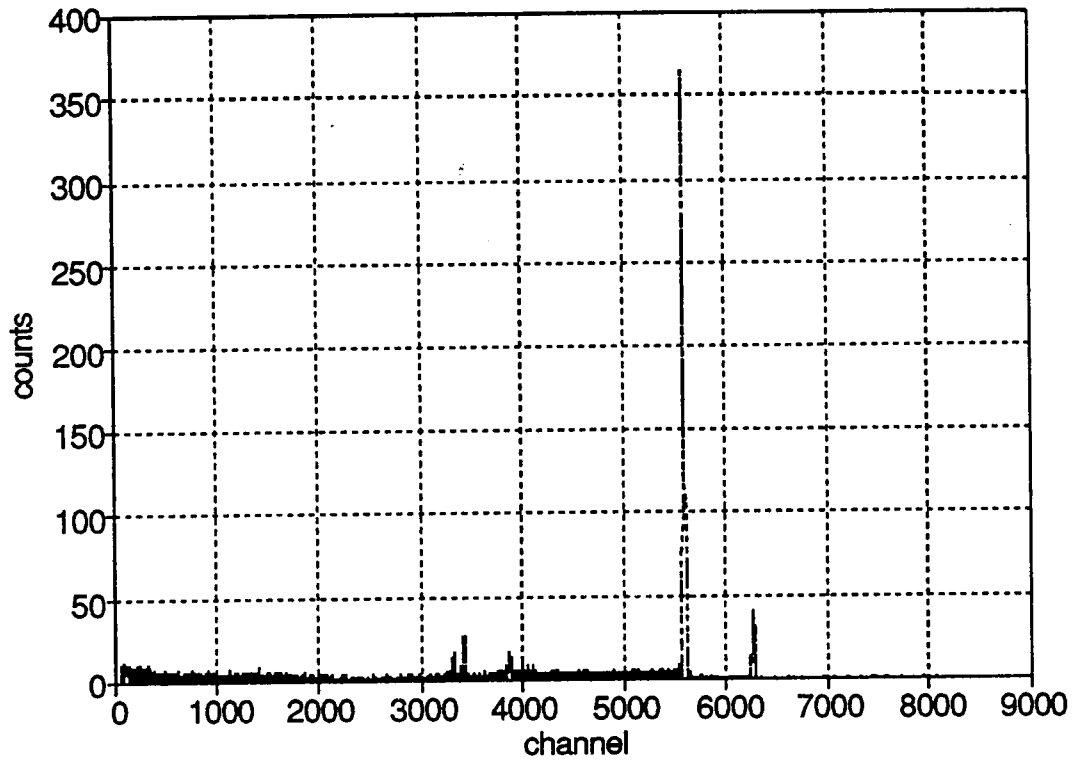

Figure 6. Cobalt-57 Spectra Used for Channel to Energy Conversion of Spectrometer Data

in Figure 5 results in the spectrum in Figure 7 which is the tube spectral intensity in counts as a function of energy in KeV.

3. DISCUSSION OF RESULTS

The X-ray tube spectra in Figure 7 differed from what was expected. The spectra shown appeared to have a characteristic line at 51.9 KeV and had a continuum of signal up to this line. The spectra should have a continuum with a maximum energy corresponding to the kilovolts readings for the accelerating potential (125 KV). Since the target material was tungsten, it should have a prominent Kα1 line at 59 KeV, a Kα2 line at 58 KeV, a Kβ1 line at 67 KeV, and a Kβ2 line at 69 KeV. These energies were derived from the energy levels in Weast [11] and were also given in Woldseth [7]. The relative intensities of the principle lines are given in Bertin [6]. The difference in the major peak at 51.9 KeV and the location of the tungsten Kα line at 59 KeV raised questions about the validity of the cobalt-57 calibration applied to the tube spectrum. The validity of using the cobalt-57 source spectra was in doubt for three reasons. First, the cobalt peaks at 122 and 136 KeV are the most visible as shown in Figure 6. To get the calibration at the lower energies, this must be extrapolated well outside this range. Second, the 136 peak in the calibration scan

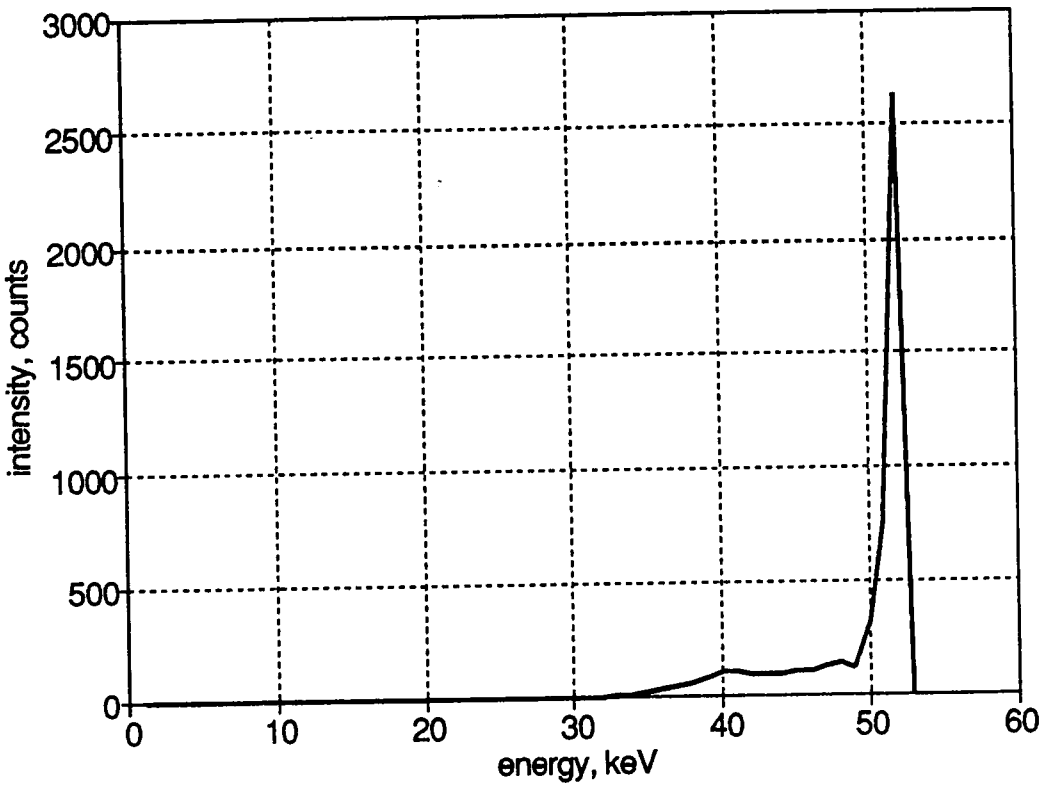

Figure 7. Experimental Source Spectra After Channel to Energy Conversion

was relatively broad, causing further concerns with the extrapolation. Third, the channel-to-energy calibration was assumed to be linear, which could be checked if more peaks were visible. This linearity could have been checked if other isotopes had also been used for calibration sources. Both ytterbium-169 and thulium-170 have spectral lines in this energy range, but were not available. If the peak was assumed to be at 59 KeV instead of 51.9 KeV, and the channel-to-energy calibration process was reversed, the 136 KeV peak should be at channel 6320. The 136 KeV peak did not begin on the cobalt scan until channel 6307. So the width of the peak did not totally explain the location of the tungsten peak, but it is close to being believable.

B. IMAGE DATA

The experimental setup for obtaining the experimental image profile was similar to that in Figure 1. The x-ray source used was a Gemini 2000™, 320 KeV source manufactured by the Ball Corporation®. This differed from the source used in gathering the source spectra only because of equipment availability. Both sources had unfiltered beryllium windows, tungsten targets, similar spot sizes, and were operated at the same voltage and current, so their output spectra should be comparable. The test object radiographed was a concentric aluminum

cylinder having an inside diameter of 3-7/16 inches and a wall thickness of 3/16 inches. The intensifying screens were zinc cadmium sulfate (ZnCdS or PFG™). The image was recorded while the source operated at 125 KeV and 1.5 mA. The image data was stored on video tape and then digitized using a Matrox® frame grabber. A gray level magnitude or intensity profile through the center of the cylinder was then taken and stored as an ASCII file. The Matrox board was an eight-bit device so the intensity values range from zero to 255 or $(2^8 - 1)$. The intensity profile is shown in Figure 8. The intensity dropped at the edges of the profile because of the angular variation of the source output. This effect was prevalent even though the entire image is within the manufacturer's specified beam angle.

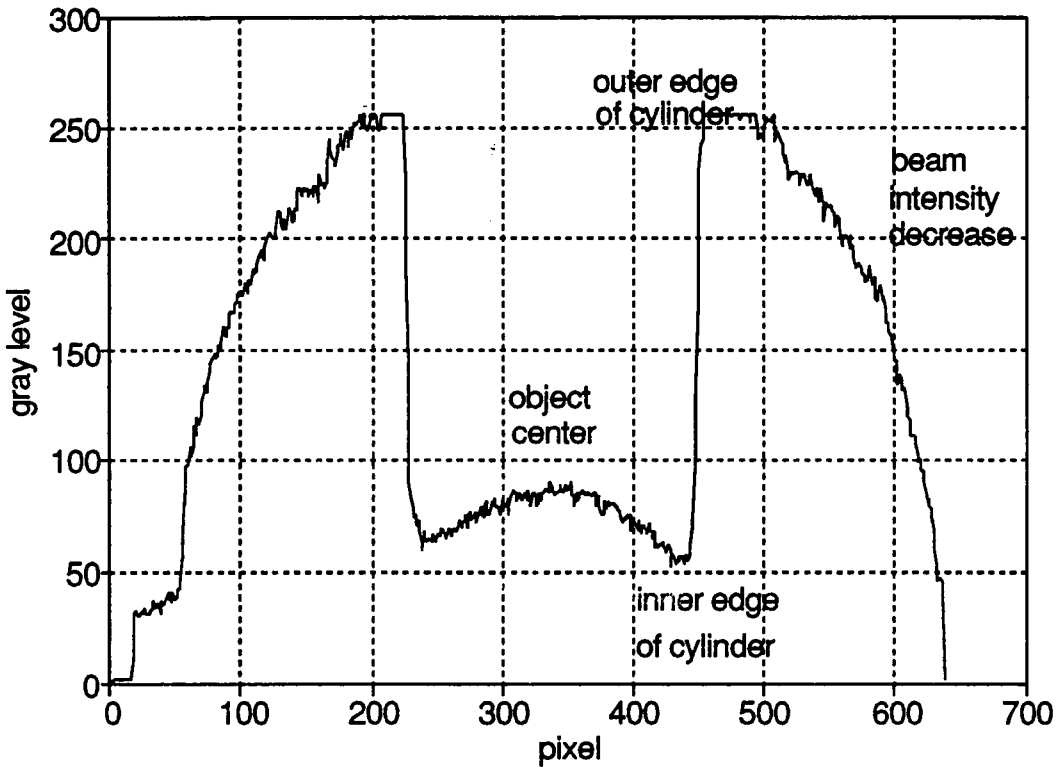

Figure 8. Image Gray Level Profile on Experimentally Derived Radiograph

IV. THEORETICAL IMAGE PREDICTION

The method used to determine the effects of energy dependence on radiographs was to generate theoretical profiles of received intensities using both monochromatic and polychromatic conditions and comparing these results to the profile from the actual radiograph. Two programs were written to predict these profiles. Mono.c is for the monochromatic condition and Poly.c is for the polychromatic condition. Both were written in the C programming language and run on a 80386 computer with the MS-DOS™ operating system. The test object for the comparison was also a hollow aluminum cylinder, but the code was written to be able to analyze the profile through a carbon cylinder as well.

A. MATHEMATICAL BASIS

Both programs were used to calculate the received intensity of the x-rays at the screens using Beer's Law for the losses in the material and free space path loss given by the equation:

$$\frac{Io}{Ix} = \frac{(dx)^2}{(do)^2} \qquad \text{(IV.1)}$$

where I_o was the intensity at a reference distance d_o, and I_x was the intensity at a distance d_x. This is also

commonly referred to the R-squared loss. The basic input files for both programs are identical and contain layout dimensions, number of pixels in the profile, and the atomic number of the target material in the anode of the source. The coordinate system and approach to finding the path lengths traveled by the beam were adopted from Frederick and Williams [1]. The coordinates are shown in Figure 9. The point of intersection of the beam with the screen, at point x_t, is given by:

$$x_t = (s + t) \tan \theta \qquad \text{(IV.2)}$$

The distance the beam travels to the screen is given by:

$$R_s = (s + t) / \cos \theta \qquad \text{(IV.3)}$$

For this ray shown

$$\sin \theta = x_t / R_s \qquad \text{(IV.4)}$$

In general, for any ray of length m

$$m \sin \theta = x_t \qquad \text{(IV.5)}$$

and

$$\cos\theta = (y + s) / m \quad \text{or} \quad y = (m \cos \theta) - s \qquad \text{(IV.6)}$$

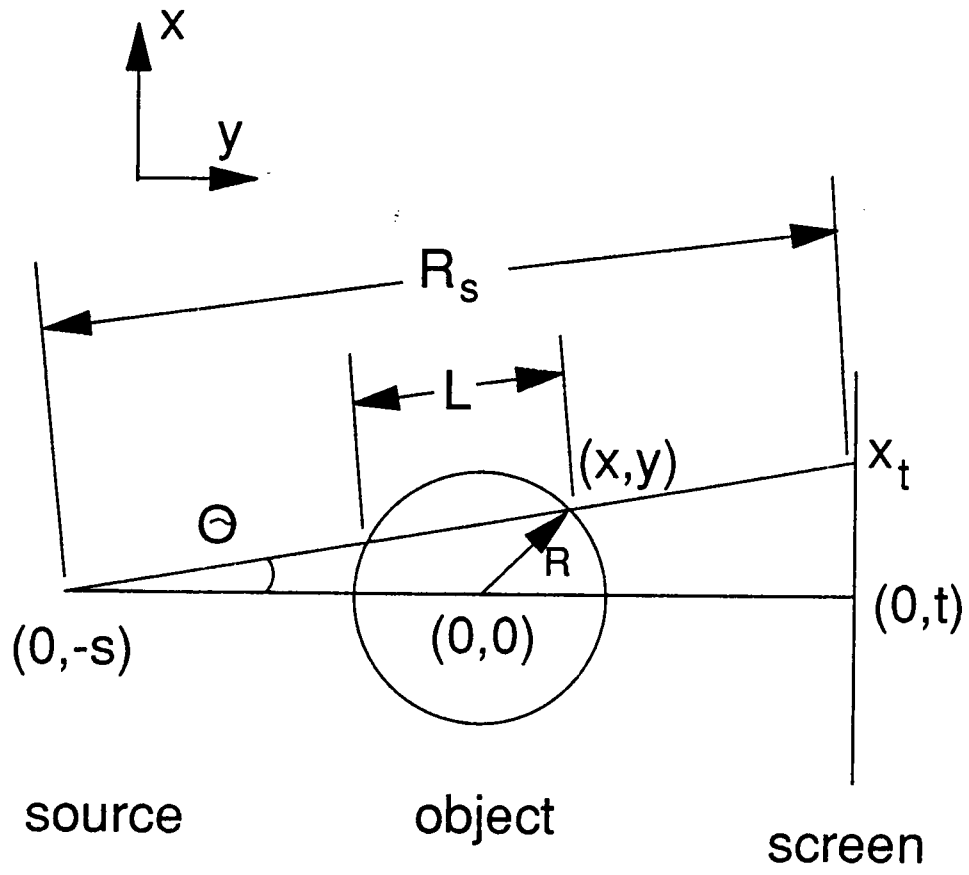

Figure 9. Coordinates for Profile Prediction Programs

The ray passes through the cylinder if x and y each have two values when results x and y of Equations IV.5 and IV.6 are substituted into the following equation:

$$x^2 + y^2 = R^2 \qquad \text{(IV.7)}$$

When these are substituted, we end up with a quadratic in the form:

$$Am^2 + Bm + C = 0 \qquad \text{(IV.8)}$$

so

$$m = \frac{-B \pm \sqrt{B^2 - 4AC}}{2A} \qquad \text{(IV.9)}$$

This yields three possible cases:

(1) If m is double valued, the ray intersects the cylinder and the solution to the equation yields the intersect points (x1,y1) and (x2,y2).

(2) If m is single valued, the ray is tangent to the cylinder.

(3) If m is complex, or $B^2 - 4AC < 0$, the ray misses the cylinder.

The equation is solved at each pixel, or x_t value. When the ray intersects the cylinder, the path length, L, through the cylinder is:

$$L^2 = (x2 - x1)^2 + (y2 - y1)^2 \qquad \text{(IV.10)}$$

The same rationale applies for the case of concentric circles but the intersection of both cylinders must be determined as in the above three cases. Two radii are supported in the Mono.c and Poly.c programs to provide for the test case of a hollow cylinder. The specifics of the programs are discussed below.

B. DESCRIPTION OF MODELS

1. Mono.c - Monochromatic Model

The computer program flowchart for the monochromatic case is shown in Figure 10. After the program reads the input file, the operator enters the source voltage (KV) setting and the output intensity in Roentgens per minute measured at a distance of one meter. The KV setting is the maximum energy being generated by the tube. The effective energy is calculated by taking two-thirds of the maximum energy. Bertin [6] states that the effective energy of the continuum is the single energy having substantially the same absorption in a given absorber as the continuum and that this energy is approximately two-thirds of the maximum. The object's mass attenuation coefficient is calculated at this effective energy using a curve fit based on data from Grodstein [12] which lists mass attenuation coefficients versus energy for a variety of

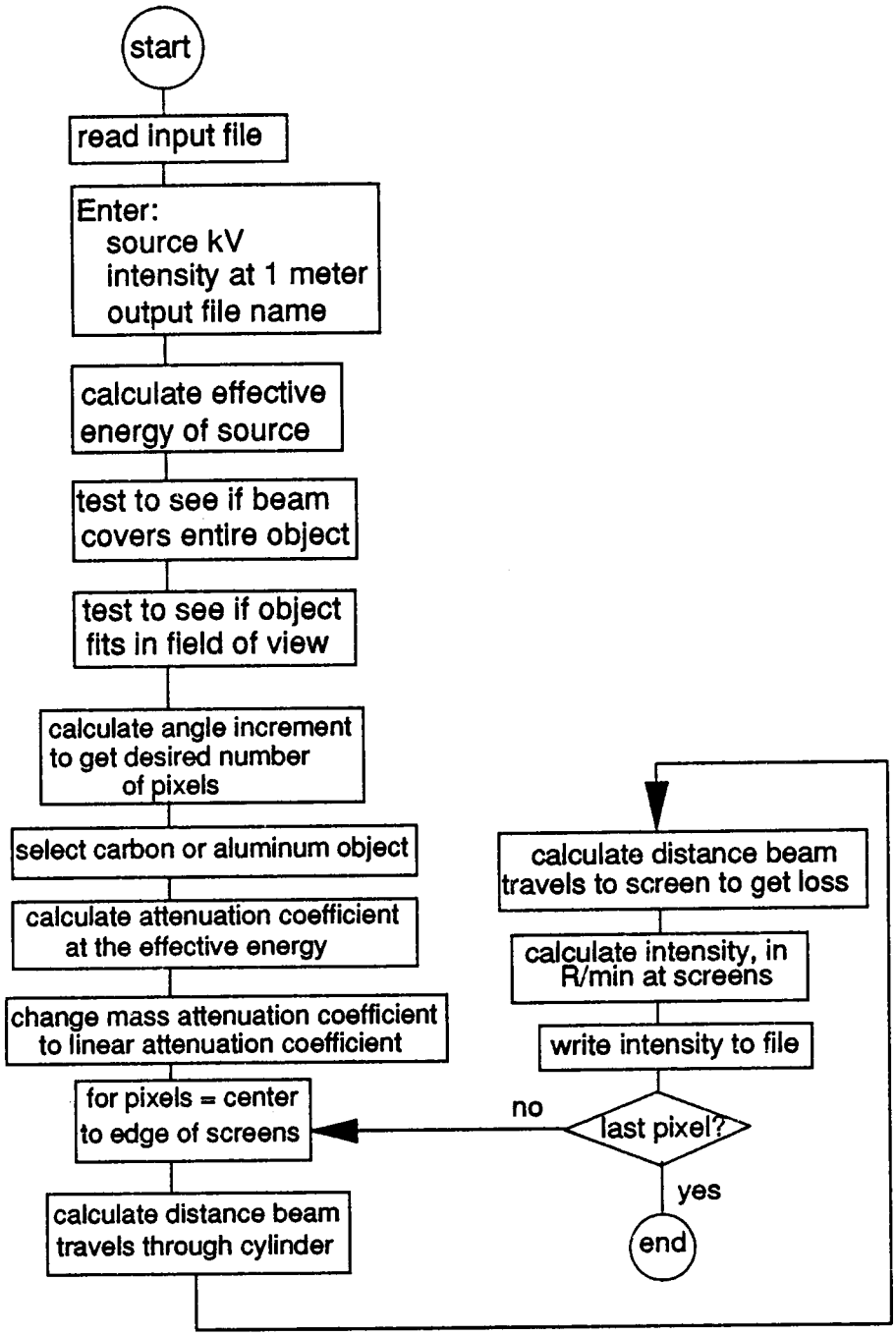

Figure 10. Monochromatic Prediction Program Flowchart

materials. This mass attenuation coefficient for the effective energy is then converted to the linear attenuation coefficient by multiplying it by the material's density. The intensity at the screens is then calculated using Beer's Law and the R-squared losses with the path lengths being calculated as above. This final intensity is given in the units of Roentgens per minute and plotted by pixel in the one dimensional array. The intensity units are relative and are not of great consequence since the profiles will later be compared to other profiles with relative units or counts.

2. Poly.c - Polychromatic Model

The computer program flowchart for the polychromatic case is shown in Figures 11 and 12. After the program reads the input file, the operator enters the source voltage in KV and current in milliamps (mA). The operator can then choose to use an experimentally derived or theoretically generated source output spectra of intensity verses energy in one KeV steps. The intensity, I, of the theoretical spectra is approximated by Kramer's formula [6]:

$$I(\lambda) = k\ i\ Z\ \left(\frac{1}{\lambda\ min} - \frac{1}{\lambda}\right)\frac{1}{\lambda^2} \qquad \text{(IV.11)}$$

where k is a constant of proportionality, i is the tube

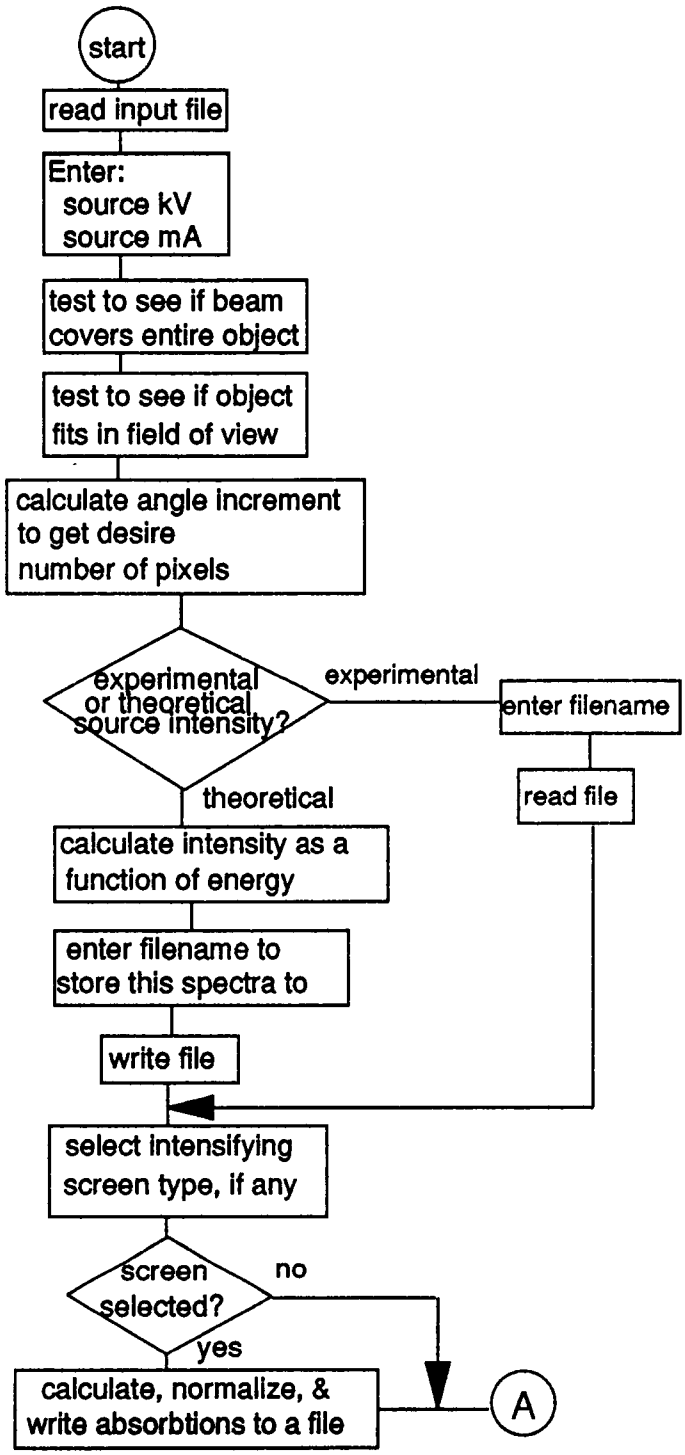

Figure 11. Polychromatic Prediction Program Flowchart

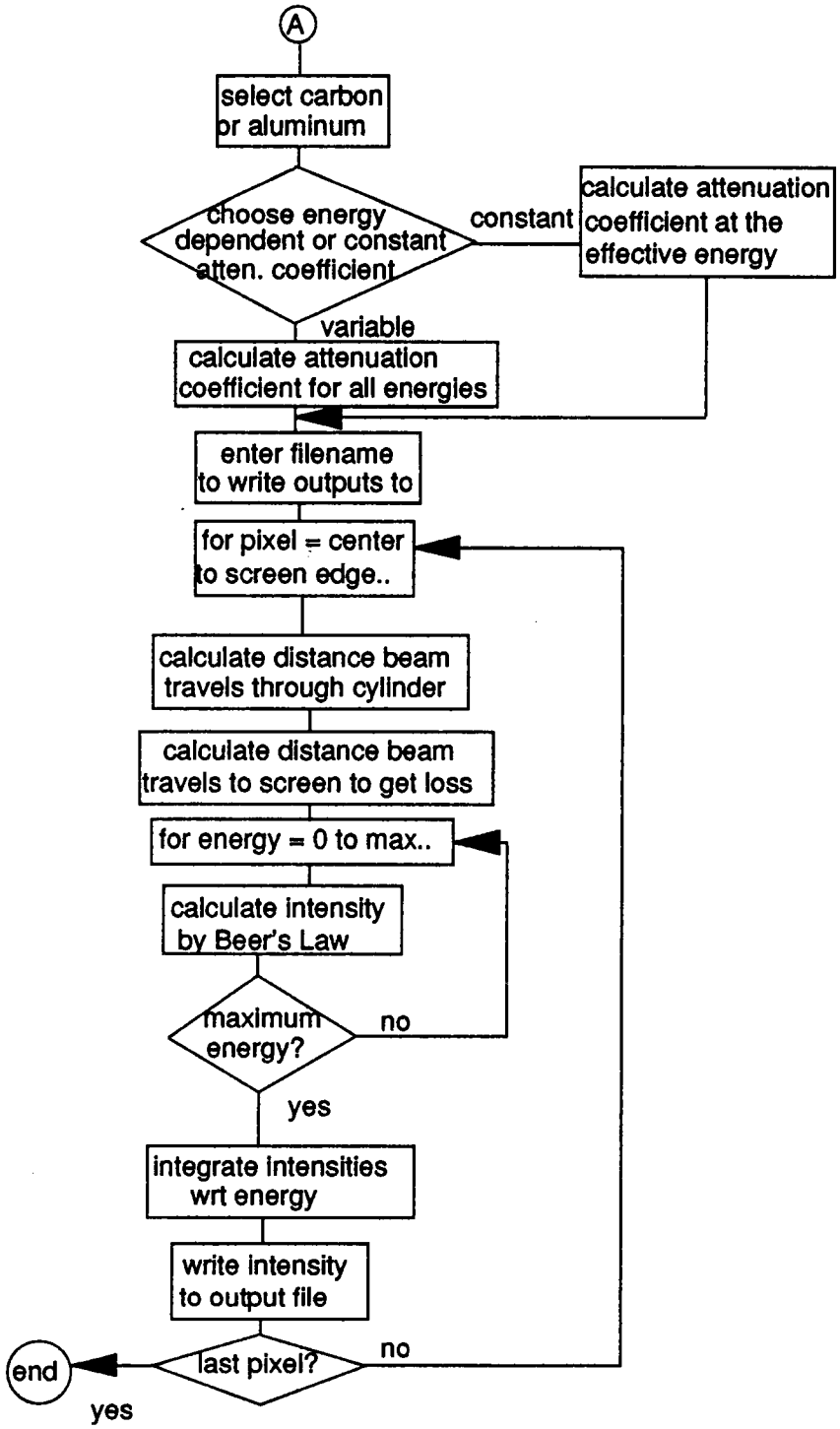

Figure 12. Continuation of Polychromatic Prediction Program Flowchart

current, Z is the atomic number, λ is the photon wavelength as in Equation II.1 and λmin is given by Equation II.2. Representative curves are plotted for several operating voltages in Figure 13. This approximation of the spectra does not include the characteristic lines. The reason that these are neglected is that even though the relative magnitudes of the characteristic lines of a spectra are well known, there is no known empirical relationship for the relative magnitudes of the characteristic lines in relation to the continuum. The operator then selects an intensifying screen type. The program allows for the following types:

1. $CaWO_4$, OPTEX ™
2. ZnS
3. $BaSO_4$
4. BaFCl
5. Y_2OS, RAREX B ™
6. LaOBr:Tb, RAREX Blue Fast ™
7. LaOBr:Tm, RAREX Blue III ™
8. $YTaO_4$:Tm
9. $YTaO_4$:Nb
10. Gd_2O_2S:Tb, RAREX Regular ™
11. La_2O_2S:Tb
12. ZnCdS:Ag, PFG ™

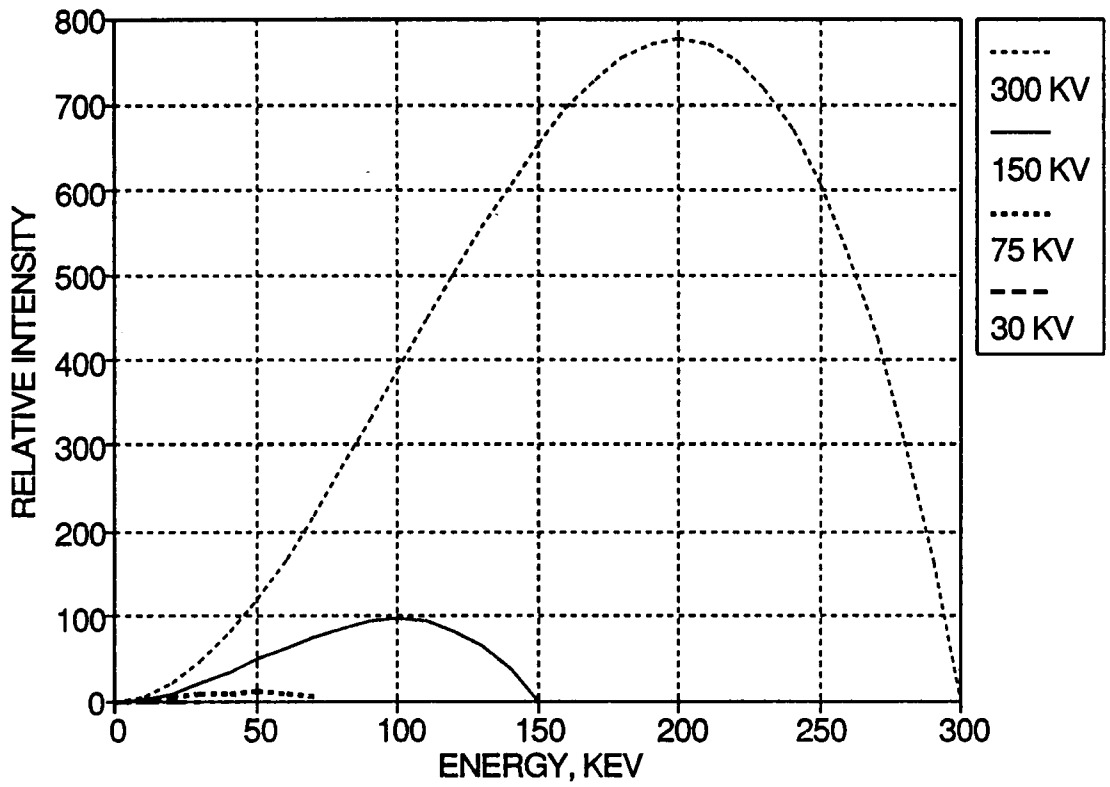

Figure 13. Continuous Spectra as Approximated by Kramer's Formula for Various Tube Voltages

13. CsI:Na

14. None

The program was used to calculate the normalized absorption curve for the selected screen. This is analogous to efficiency versus energy. These were calculated based on the absorption edge and effective atomic numbers provided by MCI Optronix®, a screen manufacturer. The screens can be considered in a similar manner to any other material, so the plot of the log of the mass attenuation coefficient versus log of the energy would yield a plot similar to Figure 3 for lead shown earlier. The curve was assumed to be linear between the absorption edges, which is reasonable in this energy range. The slope of the lines of absorption curves are generally similar for elements of similar atomic number. The effective atomic number for the screens listed vary from 26.7 to 61.8 with the average being 49.3 with a standard deviation of 11. The slope of the line was therefore approximated by that of tin ($Z_{Sn} = 50$). The amount of increase in the log of the mass attenuation coefficient at the absorption edges in this energy range is usually on the order of 0.9. Based on the derived slope, absorption edge locations, and amount of increase at the edges, the efficiency curves could then be approximated. To do this, an endpoint for the line, in

this case at one KeV, was first assumed, the curve calculated, and then normalized. Figure 14 shows the results of these calculations for two screens of interest. These were of interest because bare PFG screens were readily available for the experimental work and CsI is commonly used in x-ray image intensifiers. A limitation in this process for calculating screen absorption is that it does not allow for a relative efficiency between two screens, but this information was unknown. It also did not take into account the spectral output of the visible light of the screens or the corresponding video camera response. If no screen was selected, the efficiency was assumed to be unity at all energies.

The next parameter that could be energy dependent was the attenuation coefficient of the material. For the energy dependent case, a curve-fit equation from the Grodstein [12] data was used to generate the curve for energies one KeV to the maximum tube photon energy corresponding to the tube operating potential. If the constant case was selected, the attenuation coefficient was calculated from the curve-fit equation at the effective energy, two-thirds of the maximum, and used for all energies. At each pixel, the following were calculated:

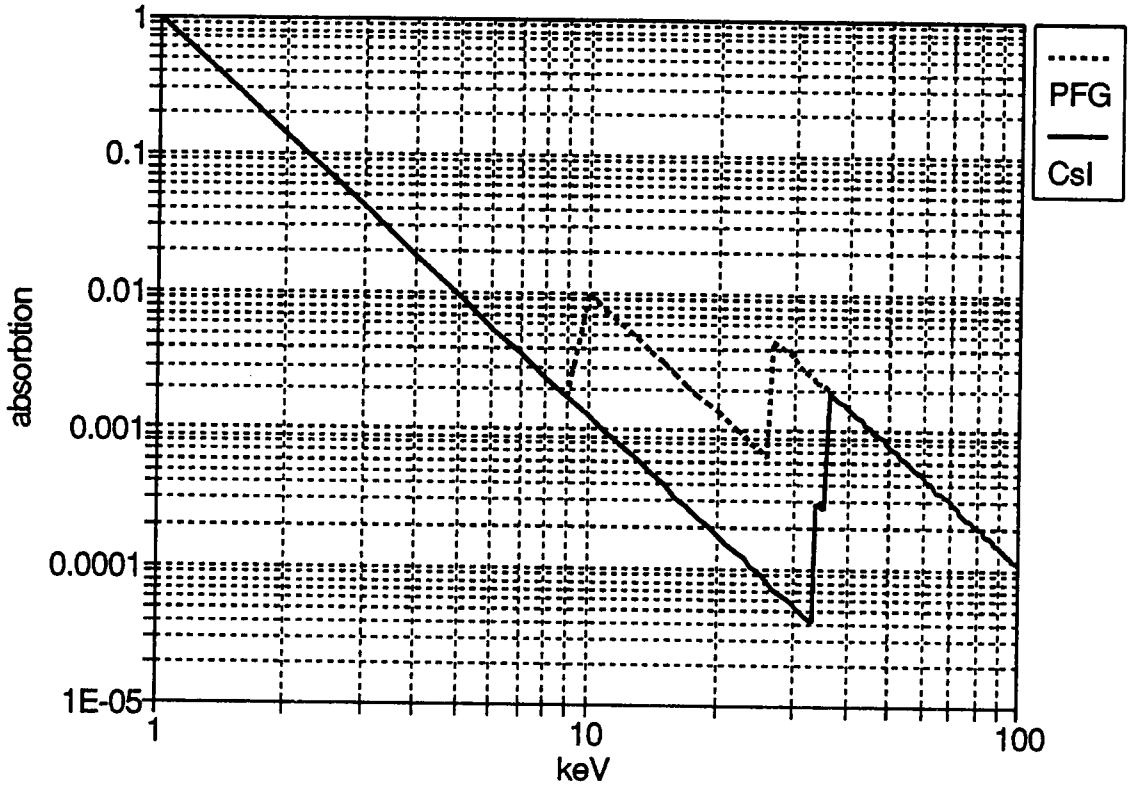

Figure 14. Normalized Screen Energy Absorptions for PFG and CsI Intensifying Screens

1. the source intensity
2. the object attenuation coefficient
3. the screen efficiency

as a function of energy for energies from one KeV to the maximum. A received intensity at each energy was then calculated using Beer's law and the R-squared losses as previously discussed, and weighted it by the screen efficiency. At each pixel, the result was an intensity as a function of energy which was then approximately integrated over the energy using Simpson's rule [13]:

$$I = h/3\ (y0 + 4y1 + 2y2 + 4y3 + 2y4 + \ldots + 2yn-4 + 4yn-3 + 2yn-2 + 4yn-1 + yn) \qquad \text{(IV.12)}$$

where I was the integral, h was the energy step size (one KeV), n was the number of data points, y. The integration yielded the final intensity at that pixel. The procedure was repeated at every pixel to produce the final intensity profile.

V. RESULTS

Figure 15 compares normalized, predicted, one dimensional intensity profiles through the centerline of a test object. The profiles were from:

a. the monochromatic model

b. the polychromatic model with the source output theoretically derived from Kramer's formula (Equation IV.14)

c. the polychromatic model with the source output as the experimental profile from the x-ray spectrometer data shown earlier in Figure 7

d. an experimentally obtained radiograph.

The test object was a hollow aluminum cylinder with a 1.5 inch inner radius and 1.7 inch outer radius and with its axis perpendicular to the incident x-rays. The source-to-object centerline distance was 28 inches and the object-to-screen distance was 12 inches. The profiles shown are only of one side of the radiograph since the object was axisymetric. The object centerline is shown at the left side of the ordinate of the graph. The monochromatic case assumed that the source spectral output, object attenuation, and screen absorption were constant functions of energy and used the measured value of 13.6 Roentgens

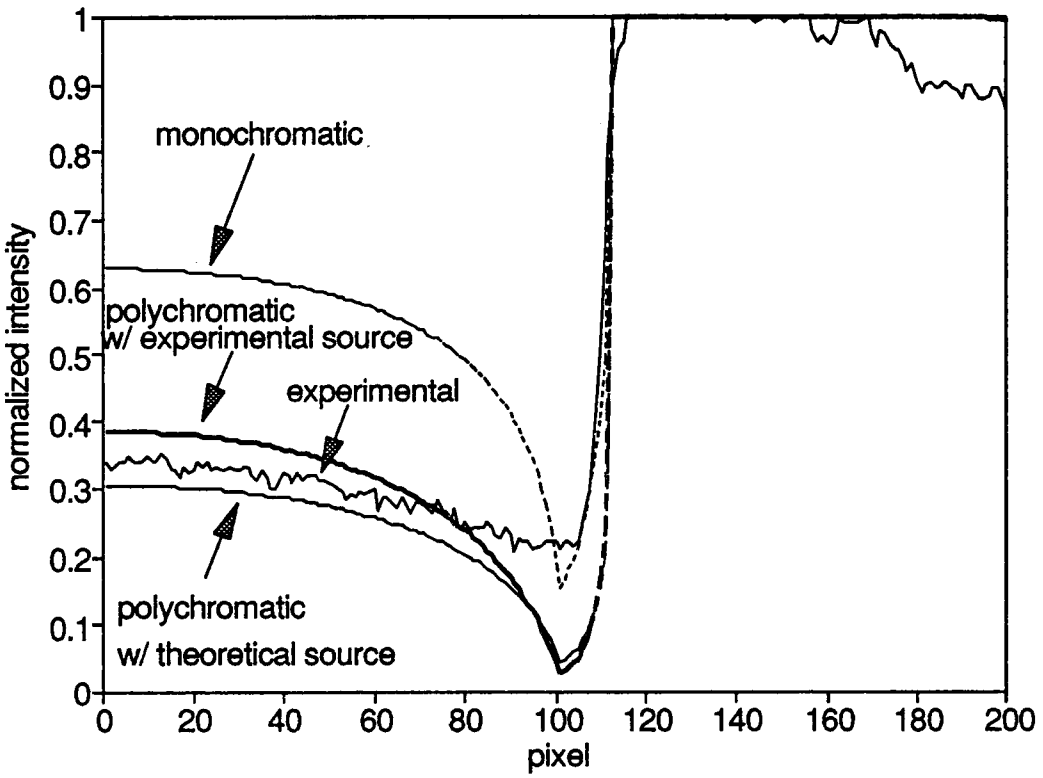

Figure 15. Theoretical Predictions vs. Experimental Profile

per minute at 125 KV as the source output. The polychromatic cases used the assumptions of variable object attenuation coefficients and PFG intensifying screens.

A quantitative comparison of the three profiles was made by computing the average percentage that the predicted profiles differed from the experimental profile over a specified pixel range. This was calculated using the following formula:

$$\frac{\sum\left(\ |\text{predicted} - \text{experimental}|\ /\ \text{experimental}\right)}{\text{number of pixels}} \qquad \text{(V.1)}$$

The number of pixels for the comparison was confined to the first 120 pixels, the area where the experimental profile did not begin to substantially roll off due to the beam angular characteristics. The monochromatic prediction varied from the actual experimentally obtained profile by 74.6 percent. The polychromatic with the theoretical source varied from the actual by 20.8 percent, and with the experimental source by 20.4 percent over this pixel range.

The shapes of all the predicted profiles in the pixel region between the inner and outer region of the cylinder have much sharper cusps than does the experimental profile. This may be due to the presence of scattering,

finite source focal spot size, and blurring due to the intensifying screens on the actual data. These effects were not modeled in the prediction programs and are more pronounced near the sharp edges of the object.

VI. DISCUSSION OF RESULTS

The results showed that in this test case the polychromatic predictions were closer to the experimentally obtained profile than was the monochromatic prediction. The major causes of the difference between the profiles were:

1) the proper effective energy of the source spectrum selected at which the monochromatic case was evaluated

2) the inability of the monochromatic prediction to consider the efficiency characteristics of the imaging medium, e.g., intensifying screens.

These effects are best explained by discussing how the profiles were generated in the polychromatic and monochromatic cases.

The general shape of a profile of a cylindrical test object is shown in Figure 16. The intensities at pixels in the A region are determined by rays not going through any material, i.e., they miss the object. The intensities at pixels in the B region are determined by rays going through some thickness of the object. Since the profile is normalized to the greatest intensity, the shape of the profile is largely determined by the relative magnitudes of the intensity at the A and B pixels. This normalization is a good approximation due to the video camera gain and

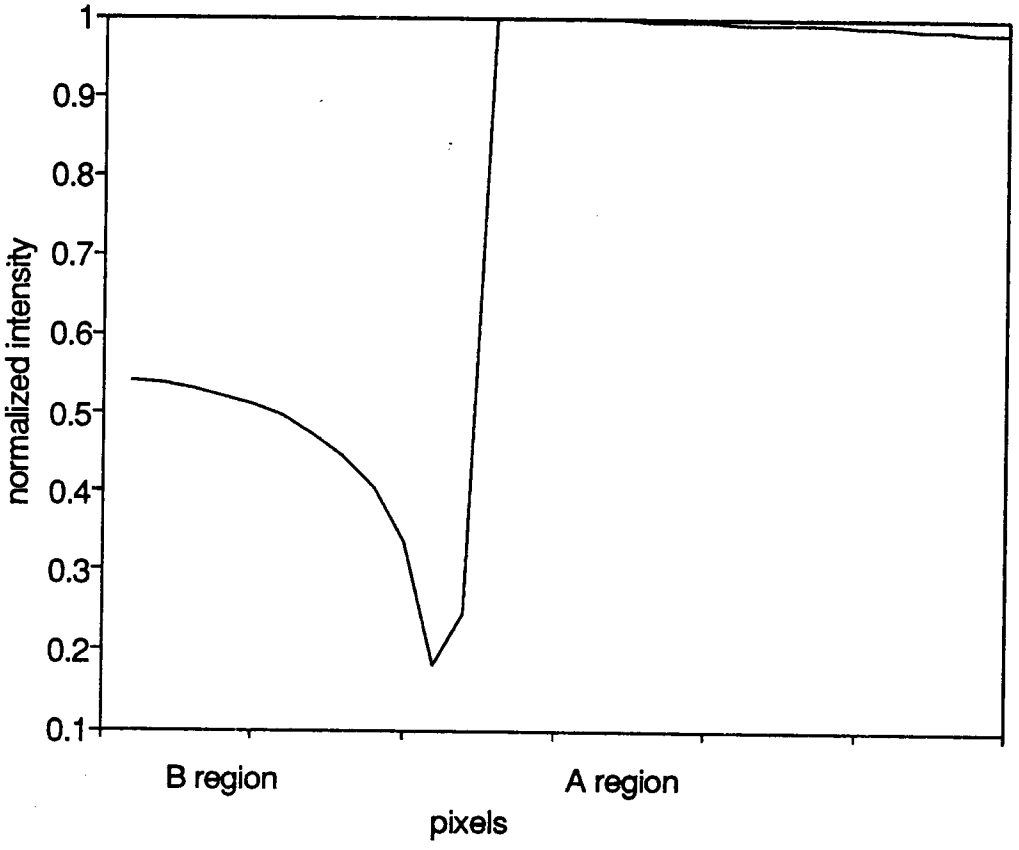

Figure 16. General Shape of an Intensity Profile of a Cylindrical Test Object

the subsequent maximization of the dynamic range of the gray levels in image during processing of the radiograph.

Neglecting the R-squared losses, the attenuation process is characterized by Beer's law for both the polychromatic and monochromatic cases. The monochromatic case is actually a special case of the polychromatic case where the energy spectrum consists of a single line at an effective energy. For the more general polychromatic case, the intensity, I_A, of the rays missing the object, or at the A region pixels is:

$$IA = \int_0^{Emax} S(E)\ Io(E)\ dE \qquad \text{(VI.1)}$$

where E is energy, S(E) is the normalized screen efficiency, $I_o(E)$ is the source output intensity, and E_{max} is the tube potential. The intensity of the rays passing through the material, or at the B region pixels is:

$$IB = \int_0^{Emax} S(E)\ Io(E)\ \exp[-\mu(E)x]dE \qquad \text{(VI.2)}$$

where x is the path length through the material, and $\mu(E)$ is the linear attenuation coefficient of the material. The relative intensity or ratio that characterizes the profile is then given by dividing Equation (VI.2) by Equation

(VI.1):

$$\frac{IB}{IA} = \frac{\int_0^{Emax} S(E)\ Io(E)\ \exp[-\mu(E)x]dE}{\int_0^{Emax} S(E)\ Io(E)\ dE} \qquad (VI.3)$$

Evaluating this relationship for the monochromatic case, i.e., for a single line spectrum at an effective energy, Eeff, yields:

$$\frac{IB}{IA} = \exp[-\mu(Eeff)\ x] \qquad (VI.4)$$

Equation VI.4 shows that the relative intensity values in the profile produced by the monochromatic prediction are affected only by the attenuation characteristics of the material itself because both the screen efficiency S(E) and the source output Io(E) terms in Equation VI.3 cancel.

For a given thickness x, there should be an effective energy where the polychromatic ratio in Equation VI.3 is equal to the monochromatic ratio in Equation VI.4. If an appropriate effective energy is chosen, the monochromatic case can approximate the polychromatic case for some usable range of material thickness. For example,

calculating the ratio in Equation VI.3 for a unit thickness of aluminum radiographed with a 160 KeV source approximated by Kramer's formula while ignoring the R-squared losses and the screen effects yields a ratio of 0.91. This was calculated by multiplying the energy dependent functions in Equation VI.3 at each energy and integrating using Simpson's rule. Substituting this result in Equation VI.4 to equate the polychromatic and monochromatic profiles yields:

$$0.91 = \exp[-\mu(Eeff)\ x] \qquad \text{(VI.5)}$$

The transmission through one inch of aluminum is shown in Figure 17. The transmission is equal to 0.91 at an energy of 79 KeV or approximately one-half of the maximum energy. This differs from the two-thirds of the maximum suggested by Bertin [6]. If the path length is increased from one to five inches and the calculations repeated, the effective energy increases to 85 KeV. Therefore the effective energy is a function of the path length the beam travels through the material. This is analogous to what is commonly referred to as "beam hardening". Therefore it is not possible to choose a single energy and produce a monochromatic profile of an object having a wide variety of path lengths to obtain an accurate prediction of the image. This suggests that if the object has a small range

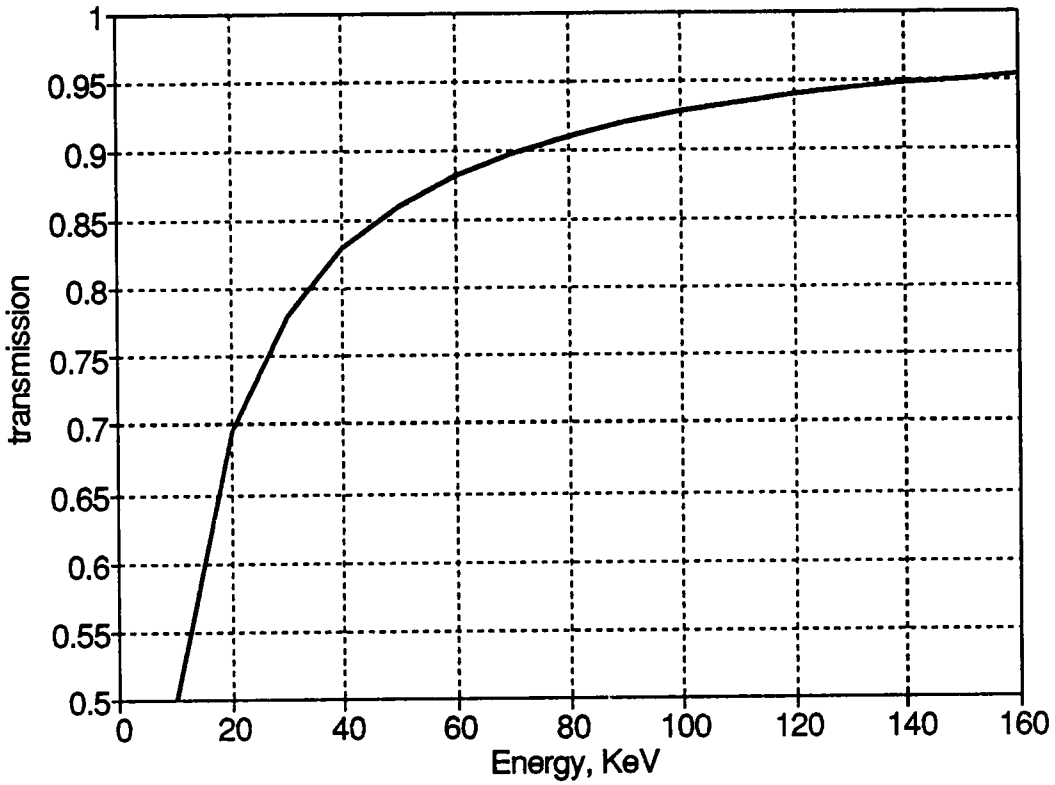

Figure 17. Transmission Factor Through One Inch of An Aluminum Object, exp(-μ)

of thicknesses, an effective energy can be calculated which when used in the monochromatic prediction, can closely approximate the polychromatic prediction. This is not the case for cylindrical or spherical objects. Figure 18 illustrates the change in the monochromatic profile evaluated at an energy of 50 percent of the maximum for this test case. The prediction varies from the polychromatic predictions as the path length through the object varies. With the adjustment in the effective energy, this profile differs from the experimental by an average of 52.5 percent instead of the earlier 74.6 percent, as evaluated using Equation V.1. This profile still differs from the experimental profile because it does not take into account the effects of the screens.

Figure 19 illustrates that the profiles from the monochromatic at an effective energy of 50 percent and the polychromatic using a theoretical spectra with no screens, are very similar. The difference in the two curves still varies with the path length. The effects of the screens can be generally quantified. If Equation VI.3 is evaluated again including the screen function, S(E) for PFG screens, the result of Equation VI.5 changes from 0.91 to 0.81. This means that the intensity through one inch of aluminum decreases by an additional 10 percent relative to the intensity at the pixels at the outside of the object. The

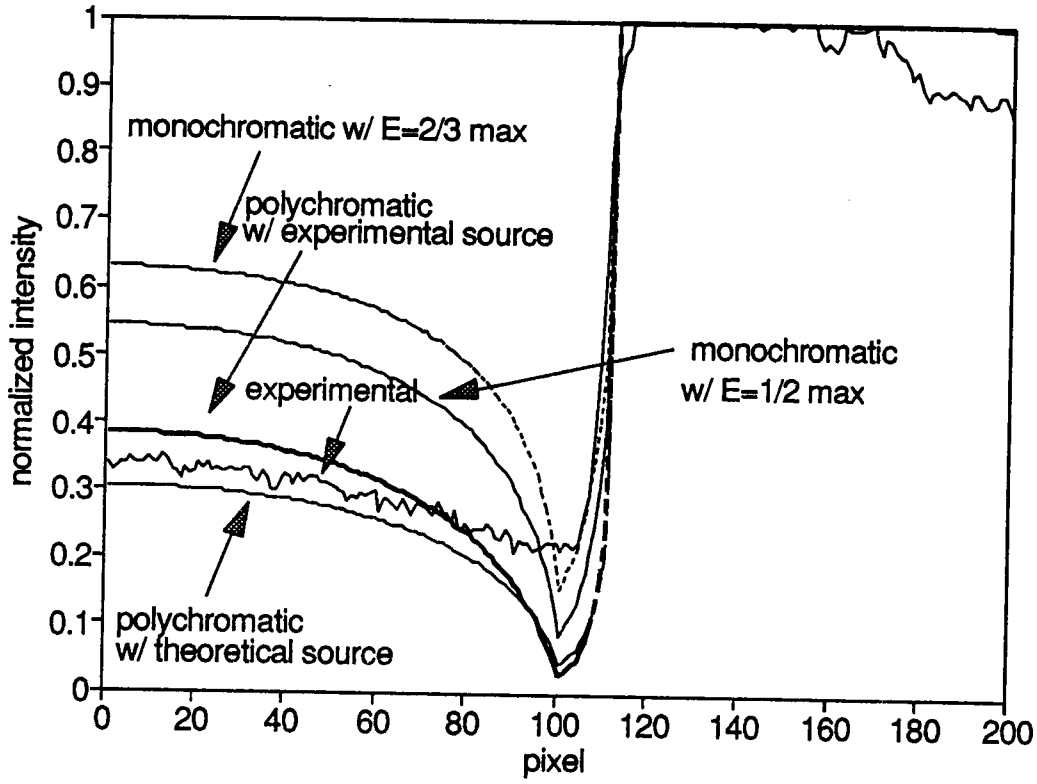

Figure 18. Monochromatic Prediction Evaluated at an Effective Energy of 50 Percent of the Tube Voltage vs. Other Profiles

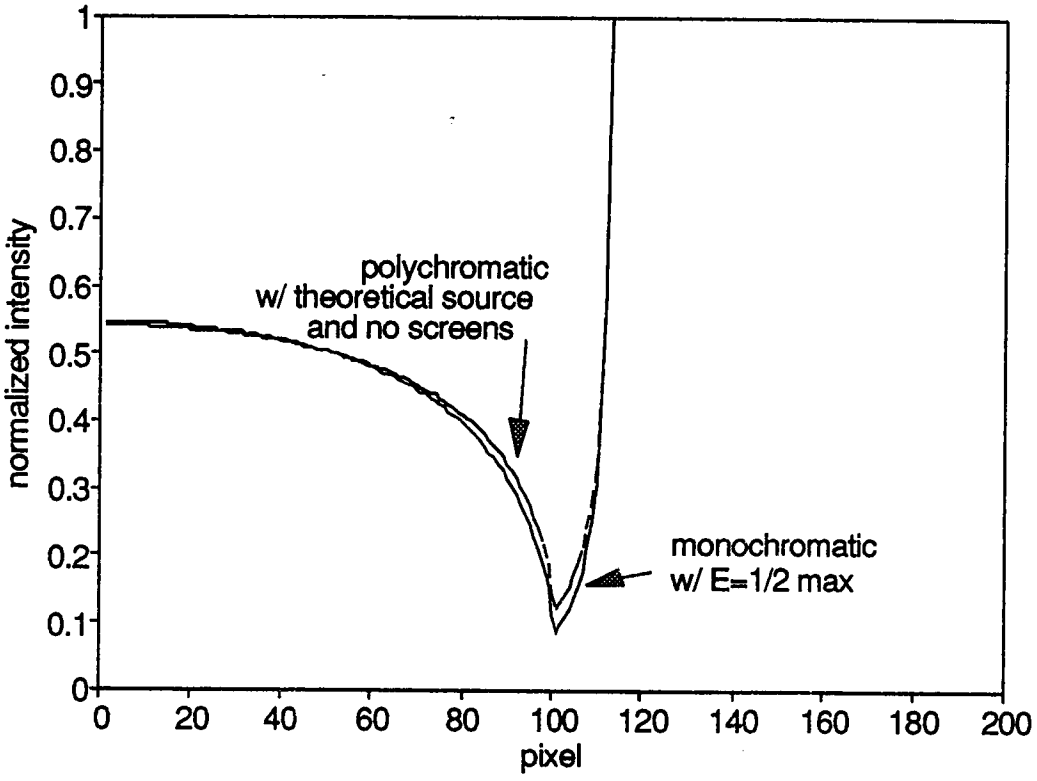

Figure 19. Monochromatic Prediction at 50 Percent Energy vs. Polychromatic Prediction With No Screens

test case illustrates that the presence of the screens can significantly affect the shape of the intensity profile.

VII. CONCLUSIONS

This work was undertaken to investigate the effects of energy dependence on X-ray radiographs for real-time radiography applications and to determine if this dependence must be considered in accurately predicting a radiograph. Computer programs were used to predict the one-dimensional intensity profiles of a radiograph of a test object. These predictions were made under the assumption that the source spectral output, object attenuation coefficient, and imaging medium, i.e., intensifying screen absorption were either monochromatic or polychromatic functions of energy. The monochromatic program was used to produce a profile with these factors evaluated at a single effective energy while the polychromatic case was used to sum the effects at all energies. These predictions were then compared to the intensity profile from an actual radiograph. The predictions made under polychromatic assumptions were significantly closer to the intensity profile on the actual radiograph. The average differences of predicted profiles from an actual profile for a cylindrical test object were calculated and are given in Table 1.

The first reason the monochromatic profile differed from the actual was that the effective energy of the x-ray source when radiographing the aluminum test object was

Table 1. Average percentage differences of predicted profiles from an actual profile for an aluminum cylinder test object.

monochromatic prediction at an effective energy of two-thirds of the maximum tube voltage	74.6
polychromatic prediction with a theoretical source spectrum approximated by Kramer's equation and PFG intensifying screens	20.8
polychromatic prediction with an experimental source spectrum from an x-ray spectrometer and PFG intensifying screens	20.4
monochromatic prediction at an effective energy of one-half of the maximum tube voltage	52.5
polychromatic prediction with a theoretical source spectrum approximated by Kramer's equation and no intensifying screens	52.5

found to differ from that prescribed by Bertin [6]. Instead of the effective energy being two-thirds of the maximum energy present, it was found to be approximately 50 percent when radiographing aluminum at 160 KeV. When the effective energy was adjusted to 50 percent of the maximum tube voltage, the intensity profile produced under monochromatic assumptions, neglecting screen effects, closely resembled that of the profile under polychromatic assumptions. The effective energy also changed as the path length through the material changed. As the path length varied by a factor of five, the effective energy varied from 49 to 53 percent of the maximum. It was concluded that if the object being radiographed had a small range of thicknesses, an effective energy could be calculated which when used in the monochromatic prediction, could closely approximate the polychromatic prediction.

The second reason the monochromatic prediction differed from the actual was that it was unable to account for the screen absorption efficiency as a function of energy. In this test case the presence of PFG intensifying screens made a significant difference in the resulting profile. A simplified analysis showed typical intensity variations of 10 percent could occur due to intensifying screens.

It is therefore concluded that the effects of energy

dependence on the radiograph be considered and that a polychromatic program be used when predicting radiographs. This program should be able to model the effects of the imaging medium. To improve on the polychromatic predictions presented here, the effects of geometric unsharpness, scattering, and relative screen visible output intensity could be incorporated into the model. The energy dependent effects of other imaging media such as film, lead screens, and glass could also be evaluated.

LIST OF REFERENCES

LIST OF REFERENCES

[1] Frederick, Robert A. and Ben M. Williams."Predicting X-rays for Dynamic Flaw Detection," JANNAF Propulsion System Hazards Subcommittee, 1991.

[2] Laguna, G.W. "An Improved Method for Simulating Radiographs," Lawrence Livermore National Laboratory, 1986.

[3] Siewert, T.A., M. W. Austin, and D.W. Fitting "Rotationally Symmeteric Image Quality Indicator for Digital X-Ray Imaging Systems," Materials Evaluation, March 1992.

[4] Cember, Herman. Introduction to Health Physics, Second Edition, Elmsford, New York: Pergamon Press, 1989.

[5] Halmshaw, R. Physics of Industrial Radiography. New York, New York: American Elsevier Publishing Company, Inc, 1966.

[6] Bertin, Eugene P. Introduction to X-ray Spectrometric Analysis. New York, New York: Plenum Press, 1978.

[7] Woldseth, Rolf. X-ray Energy Spectroscopy. San Carlos, California: Kevex Corporation, 1973.

[8] Vaughan, Douglas. Energy-Dispersive X-Ray Microanalysis, an Introduction. San Carlos, California: Kevex Instrumentents, Inc., 1989.

[9] Barrett, Harrison H. and William Swindell. Radiological Imaging, Volume One. New York, New York: Academic Press, 1981.

[10] Tipler, Paul A. Modern Physics. New York, New York: Worth Publishers, Inc., 1978.

[11] Weast, Robert C. CRC Handbook of Chemistry and Physics, 70th Edition. Boca Raton, Florida: CRC Press, Inc., 1989.

[12] Grodstein, Gladys W. "X-ray Attenuation Coefficients From 10 kev to 100 Mev," National Bureau of Standards Circular 583, 1957.

[13] Dorn, William S. and Daniel D. McCracken. Numerical Methods With Fortran IV Case Studies. New York, New York, 1972.

VITA

Michael Glenn Anderson grew up in Chattanooga, Tennessee and graduated from Hixson High School in 1979. He attended The University of Tennessee at Chattanooga and received the degree of Bachelor of Science in Engineering in 1983. After graduation he became an officer in the United States Air Force. He received the degree of Master of Science in Management from The State University of New York in Binghamton, New York in 1986. In 1988 he entered The University of Tennessee Space Institute in Tullahoma, Tennessee and in December, 1992 received a Master of Science degree in Electrical Engineering.

He is presently employed as an engineer at Sverdrup Technology, Incorporated at Arnold Engineering Development Center, where he is involved with real-time radiography development and applications.